

Shear jamming, discontinuous shear thickening, and fragile state in dry granular materials under oscillatory shear

Michio Otsuki^{1,*} and Hisao Hayakawa²

¹ Graduate School of Engineering Science, Osaka University, Toyonaka, Osaka 560-8531, Japan

² Yukawa Institute for Theoretical Physics, Kyoto University,
Kitashirakawaoiwake-cho, Sakyo-ku, Kyoto 606-8502, Japan

(Dated: December 15, 2024)

The linear response of two-dimensional frictional granular materials under an oscillatory shear is numerically investigated. It is confirmed that the shear storage modulus G' and the loss modulus G'' depend on the initial amplitude of the oscillation to prepare the system before the measurement. For sufficiently large initial strain amplitude, the shear jammed state satisfying $G' > 0$ is observed even if the packing fraction is below the jamming point. The fragile state is also identified as a long-lived metastable state where G' depends on the phase of the oscillatory shear. The dynamic viscosity evaluated from the shear loss modulus G'' exhibits a sudden jump similar to the discontinuous shear thickening in the fragile state.

Introduction.— Amorphous materials consisting of repulsive and dissipative particles including randomness such as granular materials, colloidal suspensions, foams, and emulsions can form solid-like jammed states. Since Liu and Nagel suggested that jammed states exist only above a critical packing fraction (the jamming point) [1], the jamming transition has attracted much attention among physicists [2, 3]. Several numerical simulations of frictionless grains support this picture and reveal various critical behaviors near the jamming point, where the pressure and the coordination number exhibit continuous and discontinuous transitions, respectively [4–6]. Continuous transitions are also observed for rheology of frictionless particles under steady shear [7–30] and oscillatory shear [31, 32].

Nevertheless, granular particles cannot be free from mutual frictions between grains, which play crucial roles in the dynamics of granular materials. Indeed, recent experiments suggest frictional grains follow a different scenario, i.e. jammed states for frictional grains are induced by shear deformation even below the critical fraction ϕ_C , which depends on the mutual friction between grains [33]. Such a transition, known as shear jamming, has been studied experimentally [34–36] and numerically [37, 38]. In Ref. [33], the shear jammed state is characterized by the percolation of an isotropic force network, while the fragile state is characterized by an anisotropic network.

It is also known that mutual frictions between grains cause drastic changes in rheological properties such as the discontinuous shear thickening (DST) [39–62], which is applied to flexible protective gears, robotic manipulators, and traction controls [63, 64]. There have been several studies focusing on the relationship between the DST and the shear jamming in suspensions of frictional grains under steady shear [54–57]. The definitions of the shear jamming and the fragile state, however, are inconsistent with each other, and the conclusion is still controversial [33, 54]. Therefore, we have to clarify the relationship

between the mechanical response and the shear jamming or the fragile state in granular materials.

To resolve the above puzzled situation, we numerically study the mechanical response of two-dimensional frictional grains near the jamming transition under oscillatory shear. We find that the linear response exhibits the shear jamming and the DST depending on the amplitude of the oscillatory shear before measuring it. The shear jammed state satisfying the storage modulus $G' > 0$ can be observed for the packing fraction $\phi < \phi_C$ above a critical strain amplitude. We also confirm that the observable region for the DST-like behavior is basically identical to that of a fragile state: a long-lived metastable state depending on the phase of the oscillatory shear.

Setup of Simulation.— Let us consider a two-dimensional assembly of N frictional granular particles. They interact according to the Cundall-Strack model with an identical mass density ρ in a square periodic box of linear size L [65]. The normal repulsive interaction force $\mathbf{F}_{ij}^{(n)}$ between the grain i and the grain j is given by $\mathbf{F}_{ij}^{(n)} = \left(F_{ij}^{(n,el)} + F_{ij}^{(n,vis)} \right) \Theta(d_{ij} - r_{ij}) \mathbf{n}_{ij}$, where $F_{ij}^{(n,el)} = k^{(n)}(d_{ij} - r_{ij})$ and $F_{ij}^{(n,vis)} = -\zeta^{(n)} \mathbf{v}_{ij} \cdot \mathbf{n}_{ij}$ with the normal spring constant $k^{(n)}$, the normal viscous constant $\zeta^{(n)}$, $d_{ij} = (d_i + d_j)/2$, $\mathbf{r}_{ij} = \mathbf{r}_i - \mathbf{r}_j$, $\mathbf{v}_{ij} = \mathbf{v}_i - \mathbf{v}_j$, $r_{ij} = |\mathbf{r}_{ij}|$, and $\mathbf{n}_{ij} = \mathbf{r}_{ij}/r_{ij}$. Here, the position, the velocity, and the diameter of the grain i are denoted as \mathbf{r}_i , \mathbf{v}_i , and d_i , respectively. $\Theta(x)$ is the Heaviside step function defined by $\Theta(x) = 1$ for $x \geq 0$ and $\Theta(x) = 0$ otherwise. The tangential contact force $\mathbf{F}_{ij}^{(t)}$ is given by $\mathbf{F}_{ij}^{(t)} = \min \left(|\tilde{F}_{ij}^{(t)}|, \mu F_{ij}^{(n,el)} \right) \text{sgn} \left(\tilde{F}_{ij}^{(t)} \right) \Theta(d_{ij} - r_{ij}) \mathbf{t}_{ij}$, where $\min(a, b)$ selects the smaller one between a and b , $\text{sgn}(x) = 1$ for $x \geq 0$ and $\text{sgn}(x) = -1$ otherwise, $\tilde{F}_{ij}^{(t)}$ is given by $\tilde{F}_{ij}^{(t)} = -k^{(t)} \delta_{ij}^{(t)} - \zeta^{(t)} \dot{\delta}_{ij}^{(t)}$, and $\mathbf{t}_{ij} = (-r_{ij,y}/r_{ij}, r_{ij,x}/r_{ij})$ with the α -component $r_{ij,\alpha}$ of \mathbf{r}_{ij} . Here, $k^{(t)}$ and $\zeta^{(t)}$ are the elastic and the viscous constants in the tangential direction, respectively. The

tangential displacement $\delta_{ij}^{(t)}$ is given by $\delta_{ij}^{(t)} = \int_{\text{stick}} dt \dot{\delta}_{ij}^{(t)}$ with the tangential velocity $\dot{\delta}_{ij}^{(t)} = \mathbf{v}_{ij} \cdot \mathbf{t}_{ij} - (d_i \omega_i + d_j \omega_j)/2$, where “stick” on the integral indicates that the integral is performed when the condition $|\tilde{F}_{ij}^{(t)}| < \mu F_{ij}^{(n,el)}$ is satisfied. Here, the angular velocity of the grain i is denoted as ω_i . To avoid crystallization, we use a bi-disperse system which includes equal number of grains of the diameters d_0 and $d_0/1.4$, respectively.

In this system, we apply an oscillatory shear along the y direction under the Lees-Edwards boundary condition with the SLLOD algorithm which stabilizes uniform shear flows [66]. As an initial state, the disks are randomly placed in the system with the initial packing fraction $\phi_I = 0.75$, and we slowly compress the system until the packing fraction reaches a given value ϕ as shown in Ref. [62]. After the compression, the shear strain is applied as $\gamma(t) = \gamma_0 \{\cos \theta - \cos(\omega t + \theta)\}$, where γ_0 , ω , and θ are the strain amplitude, the angular frequency, and the initial phase, respectively. For the initial $N_c^{(I)}$ cycles, we use $\gamma_0 = \gamma_0^{(I)}$ with the initial strain amplitude $\gamma_0^{(I)}$. After the initial shear, we apply the oscillatory shear with sufficiently small strain amplitude $\gamma_0 = \gamma_0^{(F)}$ for $N_c^{(F)}$ cycles, and measure the storage and the loss moduli in the final cycle defined by [67]

$$G' = -\frac{\omega}{\pi} \int_0^{2\pi/\omega} dt \sigma(t) \cos(\omega t + \theta) / \gamma_0^{(F)}, \quad (1)$$

$$G'' = \frac{\omega}{\pi} \int_0^{2\pi/\omega} dt \sigma(t) \sin(\omega t + \theta) / \gamma_0^{(F)}. \quad (2)$$

The shear stress σ is given by

$$\sigma = -\frac{1}{L^2} \sum_i \sum_{j>i} r_{ij,x} F_{ij,y}(t), \quad (3)$$

where $F_{ij,\alpha}$ is the α component of $\mathbf{F}_{ij} = \mathbf{F}_{ij}^{(n)} + \mathbf{F}_{ij}^{(t)}$. Here, we have ignored the kinetic part of σ because it is significantly smaller than the potential part for highly dissipative grains. Note that G' and the dynamic viscosity $\eta(\omega) \equiv G''(\omega)/\omega$ with $\gamma_0^{(I)} \leq 1.0$ are almost independent of ω and $\gamma_0^{(F)}$ for $\omega \leq 10^{-2}\tau^{-1}$ and $\gamma_0^{(F)} \leq 10^{-3}$, where $\tau = \sqrt{m_0/k^{(n)}}$ is the characteristic time of the stiffness with the mass m_0 for a grain of diameter d_0 [62]. We, thus, focus on the dependence of the shear modulus only on $\gamma_0^{(I)}$, θ , and ϕ for $\omega = 10^{-4}\tau^{-1}$ and $\gamma_0^{(F)} = 10^{-4}$. Here, the dynamic viscosity $\eta(\omega)$ is almost identical to the shear viscosity $\eta(0)$ [67]. We mainly use $N = 4000$, $k^{(t)} = 0.2k^{(n)}$, $\zeta^{(t)} = \zeta^{(n)} = \sqrt{m_0 k^{(n)}}$, $\mu = 1.0$, and $N_c^{(I)} = N_c^{(F)} = 10$. This set of parameters corresponds to the constant restitution coefficient $e = 0.043$. Note that we have estimated the isotropic jamming point $\phi_C = 0.821$. See Supplemental Material [68] for the determination of ϕ_C and its μ -dependence. We have also confirmed that G' is almost independent

of N , $N_c^{(I)}$, and $N_c^{(F)}$ for $N \geq 4000$, $N_c^{(I)} \geq 10$, and $N_c^{(F)} \geq 10$. We adopt the leapfrog algorithm with the time step $\Delta t = 0.05\tau$.

Mechanical response.— In Fig. 1, we plot the force chain network after the initial oscillatory shear for $\phi = 0.820 < \phi_C$ and $\theta = 0$ with $\gamma_0^{(I)} = 0.1, 0.12$ and 1.0 . For small initial strain amplitude ($\gamma_0^{(I)} = 0.1$), the system stays in a liquid-like state without percolating force chain networks. For $\gamma_0^{(I)} = 0.12$ and 1.0 , however, the systems have percolating force chain networks, where the network might be more anisotropic for $\gamma_0^{(I)} = 0.12$.

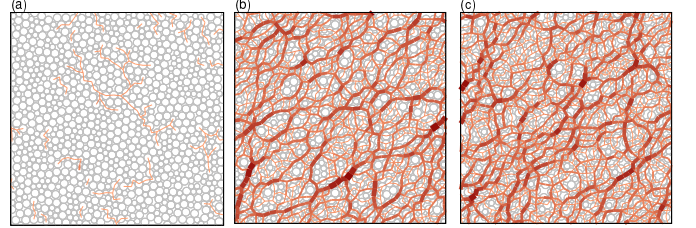


FIG. 1: Snapshots of grains (circles) and force chains (lines) after the initial oscillatory shear for $\phi = 0.820$ and $\theta = 0$ with (a) $\gamma_0^{(I)} = 0.1$, (b) 0.12 , and (c) 1.0 . The color and the width of each line depend on the absolute value of the interaction force between grains.

Figure 2 exhibits the transition from a liquid-like state to a solid-like shear jammed state, where we plot G' against $\gamma_0^{(I)}$ for $\theta = 0$ and $\pi/2$ with $\phi = 0.820$. G' changes from 0 to a finite value at a critical strain around $\gamma_0^{(I)} = 0.12$. The value of the critical strain for $G' > 0$, however, depends on θ , and the solid-like state with $G' > 0$ and the liquid-like state with $G' \simeq 0$ coexist in the shaded region of Fig. 2 as a metastable state. The inset of Fig. 2 exhibits the storage modulus G' against θ for $\phi = 0.82$ at $\gamma_0^{(I)} = 0.12$, which indicates that G' in the metastable state has peaks at $n\pi$ and becomes 0 near $(n + 1/2)\pi$ with an integer n . The stress-strain curve in the metastable state exhibits both the liquid-like and the solid-like behaviors depending on the phase of the oscillatory shear, which leads to the θ -dependence of G' . See Supplemental Material for the stress-strain curves showing the onset of the shear jamming and explaining the θ -dependence in the metastable state [68].

In Fig. 3, we plot G' against $\gamma_0^{(I)}$ for various ϕ with $\theta = 0$. For $\phi > \phi_C$, G' is finite for $\gamma_0^{(I)} = 0$, but G' depends on $\gamma_0^{(I)}$. The decrease of G' for $\phi > 0.84$ is similar to softening observed in glassy materials under steady shear [69], but G' takes a minimum value in the intermediate $\gamma_0^{(I)}$ for $0.82 < \phi < 0.84$. We confirm the existence of the shear jamming for $\phi_{SJ} < \phi < \phi_C$ with $\phi_{SJ} = 0.795$. See Supplemental Material [68] for the determination of ϕ_{SJ} . We also find the reentrant transition from finite G' to zero G' value for $\phi = 0.824$. This reentrant transition

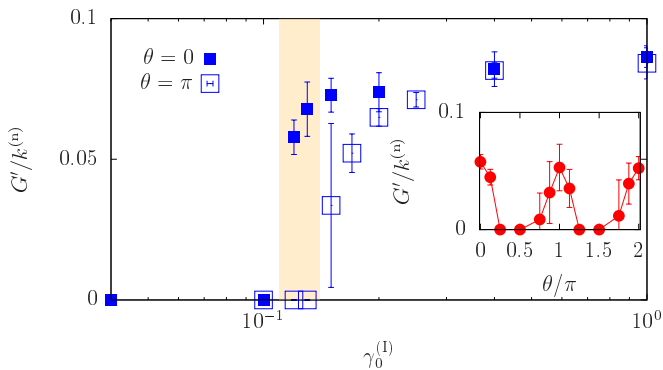


FIG. 2: The storage modulus G' against $\gamma_0^{(I)}$ for $\phi = 0.82$ with $\theta = 0$ and $\pi/2$. The shaded region indicates the fragile state. Inset: The storage modulus G' against θ for $\phi = 0.82$ with $\gamma_0^{(I)} = 0.12$

might be related to the shear jamming for frictionless grains caused by a cyclic compression [70].

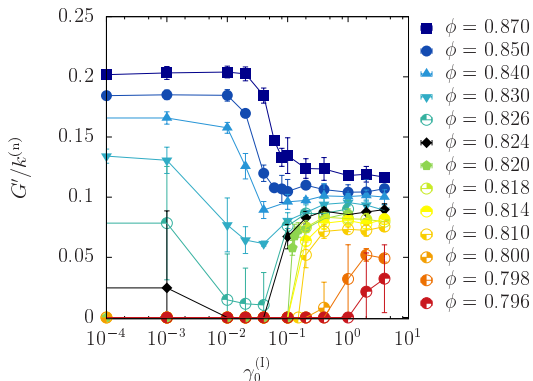


FIG. 3: The storage modulus G' against $\gamma_0^{(I)}$ for various ϕ with $\theta = 0$.

Figure 4 plots the dimensionless viscosity against $\gamma_0^{(I)}$ for $\theta = 0$ with various ϕ . For $\phi > \phi_C$, η is almost independent of $\gamma_0^{(I)}$, while η for $\phi_{SJ} < \phi < \phi_C$ exhibits a sudden increase from a negligibly small value to a larger value at a critical strain amplitude γ_{DST} . The sudden increase of η is similar to the DST under steady shear.

Phase diagram.— Figure 5 illustrates the phase diagram on the plain of $\gamma_0^{(I)}$ and ϕ . Here, we have introduced the shear storage modulus without the initial oscillatory shear: $G'_0(\phi) \equiv \lim_{\gamma_0^{(I)} \rightarrow 0} G'(\phi, \gamma_0^{(I)})$. Then, we define the jammed state (J) as the region where $G'_0(\phi) > G_{th}$ and $G'(\phi, \gamma_0^{(I)}) > G_{th}$ for any θ with a sufficiently small threshold $G_{th} = 10^{-4}k^{(n)}$. Note that the phase diagram is unchanged if we use $G_{th} = 10^{-5}k^{(n)}$. The unjammed state (U) is defined as $G'(\phi, \gamma_0^{(I)}) < G_{th}$ for any θ . The shear jammed state (SJ) is defined as $G'_0(\phi) < G_{th}$ and $G'(\phi, \gamma_0^{(I)}) > G_{th}$ for any θ . Finally, we define the fragile

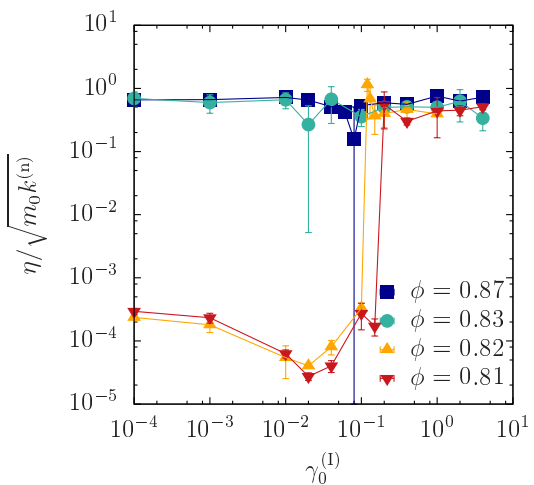


FIG. 4: The dynamic viscosity η against the initial strain amplitude $\gamma_0^{(I)}$ for $\theta = 0$ with various ϕ .

state (F) as the solid-like state with $G'(\phi, \gamma_0^{(I)}) > G_{th}$ and the liquid-like state with $G'(\phi, \gamma_0^{(I)}) < G_{th}$ coexist as shown in the shaded region of Fig. 2. In Fig. 5, SJ exists basically for $\phi_{SJ} < \phi < \phi_C$ and $\gamma_0^{(I)} > 0.1$. It is remarkable that the unjammed phase exists even for $\phi > \phi_C$, which must be related to the yielding transition, and the jammed state for intermediate $\gamma_0^{(I)}$ with $\phi > \phi_C$ located above a bay-like unjammed state might be regarded as a SJ. The unjammed state for $\phi > \phi_C$ and its relation to the yielding transition will be studied elsewhere. We have also confirmed that F exists between U and SJ. See Supplement Material [68] for the μ -dependence of SJ and the ϕ -dependence of F.

In Fig. 5, we also plot the critical strain γ_{DST} estimated from the DST-like behavior, where η exceeds a threshold $10^{-3}\sqrt{m_0 k^{(n)}}$. Note that G' also changes from 0 to a finite value at γ_{DST} . The critical strain γ_{DST} for $\theta = 0$ exists on the boundary between U and F, while γ_{DST} for other θ lies in the fragile state. This suggests that the region of the fragile state is almost identical to that for the DST-like behavior, at least, for not extremely large $\gamma_0^{(I)}$. We should note that the DST is originally defined by a jump of the viscosity against the shear rate [41], while our DST-like behavior is the discontinuous jump when we control the initial strain amplitude $\gamma_0^{(I)}$. Therefore, it is dangerous to identify DST-like behavior we have observed with the standard DST.

Discussion and concluding remarks.— Let us discuss our results. Recent numerical simulations [70–79] indicate that the shear jamming can be observed even in frictionless systems. However, the observation of SJ in frictionless systems may need special protocols such as the swap Monte Carlo algorithm [70–73], small system sizes [74–76], or the modification of the contact between grains [77–79]. These results suggest that SJ for fric-

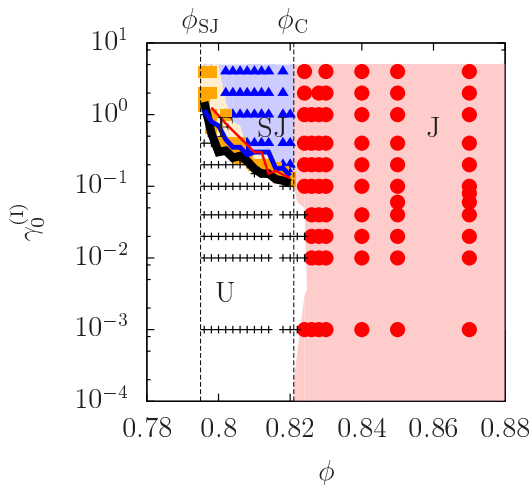


FIG. 5: The phase diagram showing different states: the jammed state (circles), the shear jammed state (triangles), the fragile state (squares), and the unjammed state (crosses). The black thick line, the blue thin line, and the red thinnest line represent the critical strain γ_{DST} for $\theta = 0, \pi/4,$ and $\pi/2,$ respectively.

tionless systems in low density regime might be unstable [77–79] and disappear in the thermodynamics limit [74–76]. This is consistent with the μ -dependence of our results shown in Supplement Material [68]. Nevertheless, some of SJ for frictionless systems might be stable only for high density regime [70–73] and related to the reentrant from the unjammed state to the jammed state for $\phi > \phi_C$ in our system. Further investigation is needed for frictionless SJ.

The fragile state is originally defined by the anisotropic percolation of the force network under quasi-static pure shear process [33]. Note that there is neither specific compression direction nor quasi-static operations in our system. Therefore, the anisotropy of the force chain network in our fragile state (Fig. 1(b)) is not clear. Nevertheless, we have confirmed that stress anisotropy τ/P , which also characterizes the onset of the shear jamming [38, 59, 76], exhibits the maximum in the fragile state and keep constant in SJ as shown in Fig. 6, where $\tau = (\sigma_1 - \sigma_2)/2$ and $P = (\sigma_1 + \sigma_2)/2$ with the maximum and the minimum principal stresses σ_1 and σ_2 , respectively. This behavior is qualitatively similar to that observed in an experiment [38]. Further careful study on the mutual relationship should be necessary.

In conclusion, we have numerically studied the frictional granular systems under oscillatory shear. Controlling the strain amplitude of the oscillatory shear before the measurement, we find that the shear jamming is regarded as a memory effect of the initial shear. This can be used to detect the DST-like behavior, where the viscosity exhibits a discontinuous jump against the initial strain amplitude. The region we observe the DST-like behavior is almost identical to that of the fragile state. Our

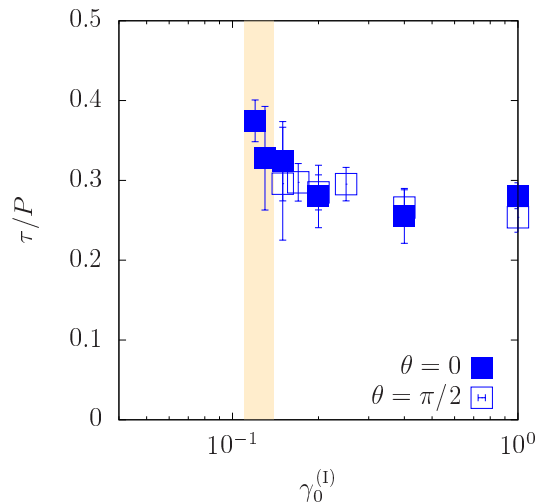


FIG. 6: The stress anisotropy τ/P against $\gamma_0^{(I)}$ for $\phi = 0.820$ with $\theta = 0$ and $\pi/2$. The shaded region indicates the fragile state.

results clarify properties of shear induced exotic states in granular materials.

The authors thank R. Behringer, B. Chakraborty, T. Kawasaki, C. Maloney, C. S. O’Hern, K. Saito, S. Sastry, S. Takada, and H. A. Vinutha for fruitful discussions. We would like to dedicate this paper to the memory of R. Behringer who has passed away in July, 2018. This work is partially supported by the Grant-in-Aid of MEXT for Scientific Research (Grant No. 16H04025 and No. 17H05420). One of the authors (M.O.) appreciates the warm hospitality of Yukawa Institute for Theoretical Physics at Kyoto University during his stay there supported by the Program No. YITP-W-15-19.

* otsuki@me.es.osaka-u.ac.jp

- [1] A. J. Liu and S. R. Nagel, *Nature* **396**, 21 (1998).
- [2] M. van Hecke, *J. Phys.: Condens. Matter* **22**, 033101 (2009)
- [3] R. P. Behringer and B. Chakraborty, *Rep. Prog. Phys.* in press.
- [4] C. S. O’Hern, S. A. Langer, A. J. Liu, and S. R. Nagel, *Phys. Rev. Lett.* **88**, 075507 (2002).
- [5] C. S. O’Hern, L. E. Silbert, A. J. Liu, and S. R. Nagel, *Phys. Rev. E* **68**, 011306 (2003).
- [6] M. Wyart, *Ann. Phys. Fr.* **30**, 3 (2005).
- [7] P. Olsson and S. Teitel, *Phys. Rev. Lett.* **99**, 178001 (2007).
- [8] T. Hatano, M. Otsuki, and S. Sasa, *J. Phys. Soc. Jpn.* **76**, 023001 (2007).
- [9] T. Hatano, *J. Phys. Soc. Jpn.* **77**, 123002 (2008).
- [10] B. P. Tighe, E. Woldhuis, J. J. C. Remmers, W. van Saarloos, and M. van Hecke, *Phys. Rev. Lett.* **105**, 088303 (2010).
- [11] T. Hatano, *Prog. Theor. Phys. Suppl.* **184**, 143 (2010).
- [12] M. Otsuki and H. Hayakawa, *Prog. Theor. Phys.* **121**,

- 647 (2009).
- [13] M. Otsuki and H. Hayakawa, Phys. Rev. E **80**, 011308 (2009).
- [14] M. Otsuki, H. Hayakawa, and S. Luding, Prog. Theor. Phys. Suppl. **184**, 110 (2010).
- [15] K. N. Nordstrom, E. Verneuil, P. E. Arratia, A. Basu, Z. Zhang, A. G. Yodh, J. P. Gollub, and D. J. Durian, Phys. Rev. Lett. **105**, 175701 (2010).
- [16] P. Olsson and S. Teitel, Phys. Rev. E **83**, 030302(R) (2011).
- [17] D. Vågberg, P. Olsson, and S. Teitel, Phys. Rev. E **83**, 031307 (2011).
- [18] M. Otsuki and H. Hayakawa, Prog. Theor. Phys. Suppl. **195**, 129 (2012).
- [19] A. Ikeda, L. Berthier, and P. Sollich, Phys. Rev. Lett. **109** 018301 (2012).
- [20] P. Olsson and S. Teitel, Phys. Rev. Lett. **109**, 108001 (2012).
- [21] E. DeGiuli, G. Düring, E. Lerner, and M. Wyart, Phys. Rev. E **91**, 062206 (2015).
- [22] D. Vågberg, P. Olsson, and S. Teitel Phys. Rev. E **93**, 052902 (2016).
- [23] F. Boyer, E. Guazzelli, and O. Pouliquen, Phys. Rev. Lett. **107**, 188301 (2011).
- [24] M. Trulsson, B. Andreotti, and P. Claudin, Phys. Rev. Lett. **109**, 118305 (2012).
- [25] B. Andreotti, J.-L. Barrat, and C. Heussinger, Phys. Rev. Lett. **109**, 105901 (2012).
- [26] E. Lerner, G. Düring, and M. Wyart, Proc. Natl. Acad. Sci. U.S.A **109**, 4798 (2012).
- [27] D. Vågberg, P. Olsson, and S. Teitel Phys. Rev. Lett. **113**, 148002 (2014).
- [28] T. Kawasaki, D. Coslovich, A. Ikeda, and L. Berthier, Phys. Rev. E **91**, 012203 (2015).
- [29] K. Suzuki and H. Hayakawa, Phys. Rev. Lett. **115**, 098001 (2015).
- [30] S. H. E. Rahbari, J. Vollmer, and H. Park, Phys. Rev. E **98**, 052905 (2018).
- [31] B. P. Tighe, Phys. Rev. Lett. **107**, 158303 (2011).
- [32] M. Otsuki and H. Hayakawa, Phys. Rev. E **90**, 042202 (2014).
- [33] D. Bi, J. Zhang, B. Chakraborty and R. Behringer, Nature **480**, 355 (2011).
- [34] J. Zhang, T. Majmudar, and R. Behringer, Chaos **18**, 041107 (2008).
- [35] J. Zhang, T. S. Majmudar, A. Tordesillas, and R. P. Behringer, Granul. Matter **12**, 159 (2010).
- [36] D. Wang, J. Ren, J. A. Dijksman, H. Zheng, and R. P. Behringer, Phys. Rev. Lett. **120**, 208004 (2018).
- [37] S. Sarkar, D. Bi, J. Zhang, R. P. Behringer and B. Chakraborty, Phys. Rev. Lett. **111**, 068301 (2013).
- [38] S. Sarkar, D. Bi, J. Zhang, J. Ren, R. P. Behringer and B. Chakraborty, Phys. Rev. E **93**, 042901 (2016).
- [39] M. Otsuki and H. Hayakawa, Phys. Rev. E **83**, 051301 (2011).
- [40] S. Chialvo, J. Sun, and S. Sundaresan, Phys. Rev. E **85**, 021305 (2012).
- [41] E. Brown and H. M. Jaeger, Phys. Rev. Lett. **103**, 086001 (2009).
- [42] R. Seto, R. Mari, J. F. Morris, and M. M. Denn, Phys. Rev. Lett. **111**, 218301 (2013).
- [43] N. Fernandez, R. Mani, D. Rinaldi, D. Kadau, M. Mosquet, H. Lombois-Burger, J. Cayer-Barrioz, H. J. Herrmann, N. D. Spencer, and L. Isa, Phys. Rev. Lett. **111**, 108301 (2013).
- [44] C. Heussinger, Phys. Rev. E **88**, 050201 (2013).
- [45] M. M. Bandi, M. K. Rivera, F. Krzakala and R.E. Ecke, Phys. Rev. E **87**, 042205 (2013).
- [46] M. P. Ciamarra, R. Pastore, M. Nicodemi, and A. Coniglio, Phys. Rev. E **84**, 041308 (2011).
- [47] R. Mari, R. Seto, J. F. Morris, and M. M. Denn, J. Rheol. **58**, 1693 (2014).
- [48] M. Grob, C. Heussinger, and A. Zippelius, Phys. Rev. E **89**, 050201(R) (2014).
- [49] T. Kawasaki, A. Ikeda, and L. Berthier, EPL **107**, 28009 (2014).
- [50] M. Wyart and M. E. Cates, Phys. Rev. Lett. **112**, 098302 (2014).
- [51] M. Grob, A. Zippelius, and C. Heussinger, Phys. Rev. E **93**, 030901(R) (2016).
- [52] H. Hayakawa and S. Takada, arXiv:1611.07295.
- [53] H. Hayakawa, S. Takada, and V. Garzo, Phys. Rev. E **96**, 042903 (2017).
- [54] I. R. Peters, S. Majumdar, and H. M. Jaeger, Nature **532**, 214 (2016).
- [55] A. Fall, F. Bertrand, D. Hautemayou, C. Mezière, P. Moucheron, A. Lemaître, and G. Ovarlez, Phys. Rev. Lett. **114**, 098301 (2015).
- [56] S. Sarkar, E. Shatoff, K. Ramola, R. Mari, J. Morris, and B. Chakraborty, EPJ Web Conf. **140**, 09045 (2017).
- [57] A. Singh, R. Mari, M. M. Denn, and J. F. Morris, J. Rheol. **62**, 457 (2018).
- [58] T. Kawasaki and L. Berthier, Phys. Rev. E **98**, 012609 (2018).
- [59] J. E. Thomas, K. Ramola, A. Singh, R. Mari, J. F. Morris, and B. Chakraborty, Phys. Rev. Lett. **121**, 128002 (2018).
- [60] E. Somfai, M. van Hecke, W. G. Ellenbroek, K. Shundyak, and W. van Saarloos, Phys. Rev. E **75**, 020301(R) (2007).
- [61] V. Magnanimo, L. La Ragione, J. T. Jenkins, P. Wang, and H. A. Makse, EPL **81**, 34006 (2008).
- [62] M. Otsuki and H. Hayakawa, Phys. Rev. E **95**, 062902 (2017).
- [63] E. Brown and H. M. Jaeger, Rep. Prog. Phys. **77**, 046602 (2014).
- [64] E. Brown, N. Rodenberg, J. Amend, A. Mozeika, E. Steltz, M. R. Zakin, H. Lipson, and H. M. Jaeger, Proc. Natl. Acad. Sci. U.S.A **107**, 18809 (2010).
- [65] P. A. Cundall and O. D. L. Strack, Geotechnique **29**, 47 (1979).
- [66] D. J. Evans and G. P. Morriss, *Statistical Mechanics of Nonequilibrium Liquids* 2nd ed. (Cambridge University Press, Cambridge, 2008).
- [67] M. Doi and S. F. Edwards, *The Theory of Polymer Dynamics* (Oxford University Press, Oxford, 1990).
- [68] See Supplemental Material.
- [69] M. Fan, K. Zhang, J. Schroers, M. D. Shattuck, and C. S. O'Hern, Phys. Rev. E **96**, 032602 (2017).
- [70] N. Kumar and S. Luding, Granul. Matter **18**, 58 (2016).
- [71] Y. Jin and H. Yoshino, Nat. Commun. **8**, 14935 (2017).
- [72] P. Urbani and F. Zamponi, Phys. Rev. Lett. **118**, 038001 (2017).
- [73] Y. Jin, P. Urbani, F. Zamponi, and H. Yoshino, arXiv:1803.04597.
- [74] T. Bertrand, R. P. Behringer, B. Chakraborty, C. S. O'Hern, and M. D. Shattuck, Phys. Rev. E **93**, 012901 (2016).

- [75] M. Baity-Jesi, C. P. Goodrich, A. J. Liu, S. R. Nagel, and J. P. Sethna, *J. Stat. Phys.* **167**, 735 (2017).
- [76] S. Chen, T. Bertrand, W. Jin, M. D. Shattuck, and C. S. O'Hern, *Phys. Rev. E* **98**, 042906 (2018).
- [77] H. A. Vinutha and S. Sastry, *Nat. Phys.* **12**, 578 (2016).
- [78] H. A. Vinutha and S. Sastry, *J. Stat. Mech.* **2016**, 094002 (2016).
- [79] H. A. Vinutha and S. Sastry, arXiv:1705.10109.

Supplemental Material:

INTRODUCTION

In this Supplemental Material, we present the stress-strain curves in the shear jammed and the fragile states, the dependence of the transition points on the friction coefficient μ , and the ϕ -dependence of the fragile state.

STRESS-STRAIN CURVES IN THE SHEAR JAMMED AND THE FRAGILE STATES

In this section, we show the stress-strain curves to illustrate how the shear jamming takes place in the initial oscillatory shear. We also explain the origin of the θ -dependent G' in the fragile state from the stress-strain curves. In Fig. S1, we plot the shear stress σ against the strain γ for $\gamma_0^{(1)} = 0.2$ with $\phi = 0.820$ and $\theta = 0$. Note that $\gamma_0^{(1)} = 0.2$ corresponds to the shear jammed states. Until γ reaches a certain value around $\gamma = 0.02$, σ remains 0. This means that the system stays in a liquid-like state because G' is zero in the linear response regime. On the other hand, σ follows a stress-strain loop once γ exceeds $\gamma \simeq 0.02$. After the initial oscillatory shear, the residual stress remains as shown in the solid square in Fig. S1, and the gradient of σ around $\gamma = 0$ indicates $G' > 0$ corresponding to the shear jamming.

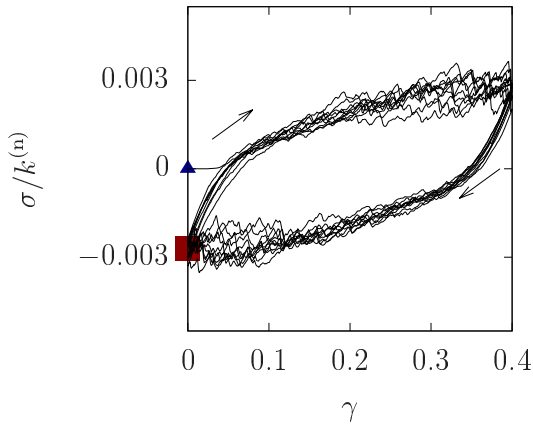
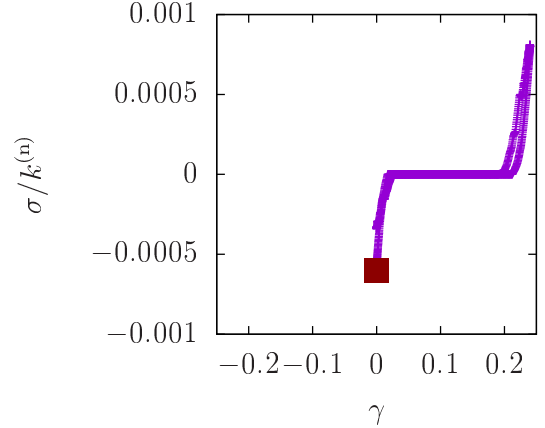


FIG. S1: The shear stress σ against the strain γ with $\gamma_0^{(1)} = 0.2$ for $\phi = 0.820$ and $\theta = 0$. The triangle and the square indicate the states before and after the initial oscillatory shear, respectively. The arrows demonstrate the evolution of σ .

Figure S2 illustrates the shear stress σ against the strain γ in the final cycle of the initial oscillatory with $\gamma_0^{(1)} = 1.2$ and $\phi = 0.820$ for $\theta = 0$ and $\pi/2$. For $\theta = 0$, σ exhibits a linear dependence on γ near the maximum and the minimum values of γ , though σ remains 0 for $0.03 < \gamma < 0.2$. Thus, the linear response after the re-

duction of the strain amplitude is solid-like i.e. $G' > 0$ near $\gamma \approx 0$. For $\theta = \pi/2$, the stress-strain curve of the initial oscillation is shifted without changing its shape. The linear response for $\theta = \pi/2$ after the reduction of the strain amplitude is liquid-like near $\gamma \approx 0$ i.e. $G' = 0$ because of the shift of the stress-strain curve. These behaviors explain the dependence of G' on θ in Fig. 2 of the main text.

(a)



(b)

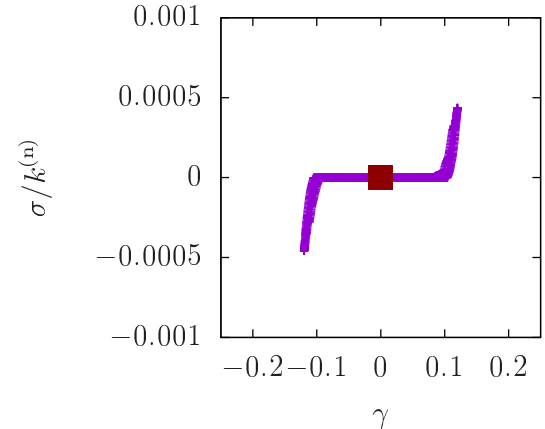


FIG. S2: The shear stress σ against the strain γ in the last cycle of the initial oscillatory with $\gamma_0^{(1)} = 0.12$ at $\phi = 0.820$ for $\theta = 0$ (a) and $\pi/2$ (b). The solid squares indicate the positions to measure the linear response after the reduction of the strain amplitude.

DEPENDENCE OF TRANSITION POINTS ON μ

In this section, we discuss the dependence of transition points ϕ_C and ϕ_{SJ} . In Fig. S3, we plot the storage modulus G' against ϕ for $\theta = 0$ with various $\gamma_0^{(1)}$. For every $\gamma_0^{(1)}$, G' exhibits an almost discontinuous transition. Note that the transition point depends on $\gamma_0^{(1)}$ and θ . We,

thus, introduce the critical fraction $\phi_{\text{th}}(\gamma_0^{(I)}, \theta)$ as a packing fraction where G' exceeds $G_{\text{th}} = 10^{-4}k^{(n)}$. Then, we define the jamming transition point for isotropic packings as

$$\phi_C \equiv \lim_{\gamma_0^{(I)} \rightarrow 0} \phi_{\text{th}}(\gamma_0^{(I)}, \theta), \quad (\text{S1})$$

which does not depend on θ . We also define the minimum critical fraction for solid-like states as

$$\phi_{\text{SJ}} \equiv \min_{\gamma_0^{(I)}, \theta} \phi_{\text{th}}(\gamma_0^{(I)}, \theta). \quad (\text{S2})$$

Note that $\phi_{\text{th}}(\gamma_0^{(I)}, \theta)$ has the minimum at $\theta = 0$, and decreases with increasing $\gamma_0^{(I)}$. We, thus, evaluate ϕ_{SJ} by the extrapolation of $\phi_{\text{th}}(\gamma_0^{(I)}, \theta)$ in the limit $\gamma_0^{(I)} \rightarrow \infty$ with $\theta = 0$ using the data for $\gamma_0^{(I)} \leq 2.0$.

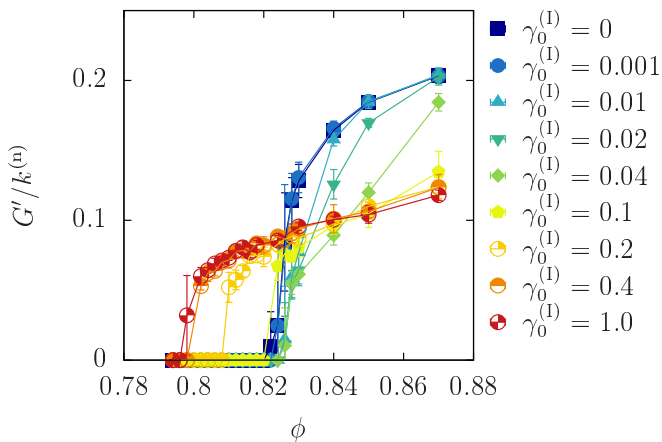


FIG. S3: The storage modulus G' against ϕ for $\theta = 0$ and $\mu = 1.0$ with various $\gamma_0^{(I)}$.

In the main text, we have discussed the case only for $\mu = 1.0$, but we investigate the μ -dependence of the critical points ϕ_C and ϕ_{SJ} in Fig. S4. Note that the shear jamming is observed for $\phi_{\text{SJ}} \leq \phi \leq \phi_C$. As shown in Fig. S4, the difference between ϕ_C and ϕ_{SJ} decreases to 0 as μ decreases, which indicates that the shear jamming we have observed disappears in the frictionless limit.

ORDER PARAMETER FOR THE FRAGILE STATE

As shown in Fig. 5 of the main text, the fragile state disappears as ϕ approaches the fraction at the tricritical point, which is almost equivalent to ϕ_C . Here, we introduce the order parameter of the fragile state for a given

ϕ as

$$\Delta\gamma(\phi) = \gamma_{\text{max}}(\phi) - \gamma_{\text{min}}(\phi). \quad (\text{S3})$$

Here, $\gamma_{\text{max}}(\phi)$ represents the boundary between SJ and F, while $\gamma_{\text{min}}(\phi)$ denotes the boundary between F and

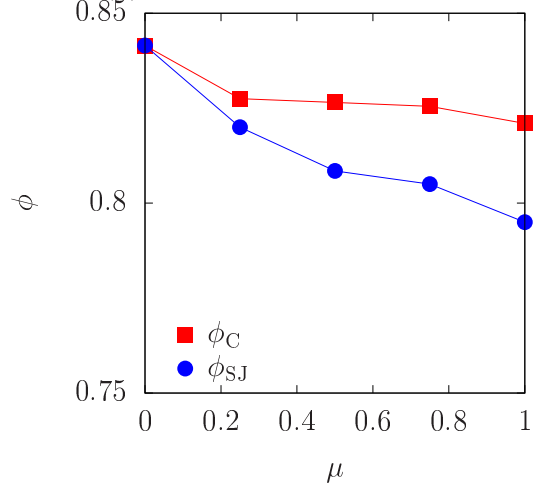


FIG. S4: The transition points ϕ_C and ϕ_{SJ} against μ .

U. In Fig. S5, we plot $\Delta\gamma$ against ϕ for $\mu = 1.0$. $\Delta\gamma$ rapidly increases as ϕ decreases from ϕ_C . This suggests that the behavior at the critical point is singular, which might be helpful to construct a mean field theory of the shear jamming transition.

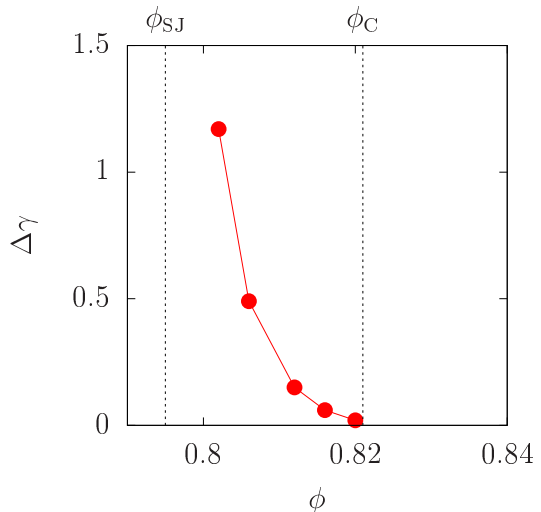


FIG. S5: $\Delta\gamma$ against ϕ for $\mu = 1.0$. Here, ϕ_C is the critical fraction for the isotropic jamming.